LIBRARY
METEOROLOGICAL OFFICE
124415
14 JUN 1977
LIBRARY

Occasional Note Met O 21/77/2

STABILITY OF FLOW IN A SLOWLY ROTATING TWO-LAYER SYSTEM

by

Ian N. James

Geophysical Fluid Dynamics Laboratory,
Meteorological Office,
Bracknell,
Berkshire.

April 1977

1. BACKGROUND TO THE PROBLEM

The motions in a rotating system in which a shear is maintained across the interface of two immiscible fluids of different density are of considerable interest in geophysical fluid mechanics, since this is one of the simplest systems to exhibit baroclinic instability or "sloping convection". When the rotation is rapid, the quasi-geostrophic equations are appropriate and the linear theory of baroclinic instability may be derived. The effects of Ekman boundary layers and sloping endwalls, etc, can be easily included (Hide, 1975). The relative simplicity of the dispersion relation in such a system has been exploited in investigations of the effect of non-linearities on baroclinic waves, and in elucidating the mechanicisms of vacillation (Lorenz 1963, Pedlosky, 1971, 1972 and Hart, 1976). Because of its theoretical simplicity, and because it is a relatively simple system mechanically, experimentalists have constructed apparatus to drive a shear across two layers of immiscible fluid (Hart, 1972, 1973), and to monitor the resulting motions as revealed by variations of the interface height.

When the system is not rotating, instability can still occur provided the shear is large enough. This instability has rather different characteristics and is a particular example of the Kelvin-Helmholtz instability. The instability is well-documented; the treatise by Chandrasekhar (1961) contains a useful introduction to the topic.

The effect of slow rotation on the Kelvin-Helmholtz instability is less well-documented, and indeed is, in its full generality, a much more difficult problem (see Chandrasekhar 1961, pp 498-506). It is probably of importance in the laboratory two-layer system, since two distinct modes of instability are observed (Williams 1976), viz, a relatively slow, long wave instability, corresponding to the baroclinic instability, and a shorter wave length, faster instability which experimenters have related to the Kelvin-Helmholtz mode of non-rotating systems.

The object of the work described in this paper is to examine this interpretation of the experimental results, and to see how the linear theory of Kelvin-Helmholtz instability is modified by rotation. Again, the possibility that linear theory might predict the co-existence of both baroclinic and "Kelvin-Helmholtz" instability for certain parameter ranges, will be considered.

Orlanski (1968), has discussed a somewhat similar problem, namely the instability of a frontal surface, and his analysis forms the basis of the present work. However, his analysis is rather more complicated since the sidewalls are taken at infinity; consequently the interface intersects the upper and lower surfaces, not the sidewalls. Furthermore, I shall include the possibility of a surface tension at the interface, an effect neglected by Orlanski. This is probably unimportant in the atmospheric context but it is important in a laboratory system in ensuring a short wave cut-off of the Kelvin-Helmholtz instability.

In the following I shall describe the equations governing the flow, and shall describe a suitable scaling of them. I shall then use a simple linear perturbation of these equations to describe the evolution of small disturbances. Before treating the general rotating case it will be helpful to discuss the non rotating case.

2. THE GOVERNING EQUATIONS

I shall consider the situation shown in figure (1); two layers of incompressible immiscible inviscid fluid pass along an infinite channel, bounded above and below by rigid boundaries at $z^* = 0^+$ and $z^* = D$, and laterally by rigid boundaries at $y^* = \pm L/2$. The densities of the two layers of fluid are ρ_1 and ρ_2 and the surface tension along the interface at $z^* = h^*$ is S. The layers of fluid move in the x-direction at velocities U_1 and U_2. In the absence of boundary layers or irregularities on the boundary surfaces there is no loss of generality in taking these velocities to be $-\Delta U/2$ and $+\Delta U/2$ respectively. The entire system is supposed to rotate about a vertical axis with angular velocity Ω .

+ Throughout this paper the asterisk superscript is used to denote dimensional variables.

The system is governed by a set of seven partial differential equations, which result from the application of conservation of mass, conservation of momentum and hydrostatic balance to the two layers.

In the ensuing analysis I shall assume that the velocity fields u_j^*, v_j^* (where j = 1 or 2 indicates the layer) are independent of z^*. It follows from the continuity equation that

$$\frac{\partial w_j^*}{\partial z^*} = -\left(\frac{\partial u_j^*}{\partial x^*} + \frac{\partial v_j^*}{\partial y^*} \right) = \text{constant.} \qquad (2.1)$$

Such an assumption can be justified using the Taylor-Proudman theorem for rapid rotation. When the rotation is slow it is simply an assumption designed to render the mathematics tractable. Comparison with experiments show that there cannot be more complicated motions which are noticeably more unstable in the parameter range attainable in the laboratory.

Consider the lower layer; variations in the depth of the layer are related to the vertical velocity at the interface:

$$\frac{Dh^*}{Dt^*} = w_1^*(h^*) = \int_0^{h^*} \frac{\partial w_1^*}{\partial z^*}\, dz^* \qquad (2.2)$$

where D/Dt^* is the **Lagrangian time derivative.**

Using equation (2.1) it is easily seen that

$$\frac{Dh^*}{Dt^*} = -h^*\left(\frac{\partial u_1^*}{\partial x^*} + \frac{\partial v_1^*}{\partial y^*} \right) \qquad (2.3)$$

and consequently that the Eulerian rate of change of interface height is

$$\frac{\partial h^*}{\partial t^*} = -\frac{\partial}{\partial x^*}(h^* u_1^*) - \frac{\partial}{\partial y^*}(h^* v_1^*) \qquad (2.4)$$

Similar considerations apply to the upper layer, and yield a second equation for $\partial h^*/\partial t^*$:

$$\frac{\partial h^*}{\partial t^*} = \frac{\partial}{\partial x^*}\left([D-h^*]u_1^*\right) + \frac{\partial}{\partial y^*}\left([D-h^*]v_1^*\right) \qquad (2.5)$$

The rate of change of velocity in either layer is given by the usual momentum equations in a rotating system:

$$\left.\begin{aligned} \frac{\partial u_j^*}{\partial t^*} + u_j^*\frac{\partial u_j^*}{\partial x^*} + v_j^*\frac{\partial u_j^*}{\partial y^*} - 2\Omega v_j^* &= -\frac{1}{\rho_j}\frac{\partial p_j^*}{\partial x^*} \\ \frac{\partial v_j^*}{\partial t^*} + u_j^*\frac{\partial v_j^*}{\partial x^*} + v_j^*\frac{\partial v_j^*}{\partial y^*} + 2\Omega u_j^* &= -\frac{1}{\rho_j}\frac{\partial p_j^*}{\partial y^*} \end{aligned}\right\} \qquad (2.6)$$

The pressure p_j^* consists of the sum of two parts of which are functions of x and y and of z respectively; only the first part contributes to equation (2.6). I shall therefore take p_1^* to be the pressure at $z^* = 0$ and p_2^* to be the pressure at $z^* = D$.

A final equation links p_1^* to p_2^*. p_1^* exceeds p_2^* because of two effects; first by the weight of overlying fluid and second by the excess pressure caused by the surface tension. Thus

$$p_1^* = p_2^* + (\rho_1-\rho_2)g h^* + \rho_2 g H - S\left(\frac{\partial^2 h^*}{\partial x^{*2}} + \frac{\partial^2 h^*}{\partial y^{*2}}\right) \qquad (2.7)$$

provided the curvature of the interface is nowhere too sharp.

Before proceeding further I shall rewrite the governing equations (2.4) to (2.7) in terms of dimensionless variables. Let L be a typical horizontal length scale and D a typical vertical length scale. A typical velocity is ΔU, and the time scale is $L/\Delta U$. H is convenient to express the densities in terms of a dimensionless parameter σ ; thus

$$\left.\begin{aligned} \rho_1 &= \bar{\rho}\,(1+\sigma/2) \\ \rho_2 &= \bar{\rho}\,(1-\sigma/2) \end{aligned}\right\} \qquad (2.8)$$

Dimensional analysis shows that a consistent scaling of the pressure is $\bar{\rho}\,\Delta U^2$. Equations (2.4) to (2.7) may now be rewritten

$$\frac{\partial h}{\partial t} = -\frac{\partial (u_1 h)}{\partial x} - \frac{\partial (v_1 h)}{\partial y} \qquad (2.9)$$

$$\frac{\partial h}{\partial t} = \frac{\partial}{\partial x}\left[u_2 (1-h)\right] + \frac{\partial}{\partial y}\left[v_2 (1-h)\right] \qquad (2.10)$$

$$\frac{\partial u_j}{\partial t} + u_j \frac{\partial u_j}{\partial x} + v_j \frac{\partial u_j}{\partial y} - \frac{1}{\epsilon} v_j = -\frac{\bar{\rho}}{\rho_j} \frac{\partial p_j}{\partial x} \qquad (2.11)$$

$$\frac{\partial v_j}{\partial t} + u_j \frac{\partial v_j}{\partial x} + v_j \frac{\partial v_j}{\partial y} + \frac{1}{\epsilon} u_j = -\frac{\bar{\rho}}{\rho_j} \frac{\partial p_j}{\partial y} \qquad (2.12)$$

$$p_1 - p_2 = \frac{g H \rho_2}{\bar{\rho}\,\Delta U^2} + Rh - T\left(\frac{\partial^2 h}{\partial x^2} + \frac{\partial^2 h}{\partial y^2}\right) \qquad (2.13)$$

where I have defined a Rossby number $\epsilon = \Delta U/(2\Omega L)$, a Richardson number $R = \sigma g D/\Delta U^2$ and $T = SD/(\bar{\rho} L^2 \Delta U^2)$. T^{-1} is sometimes known as a Weber number.

3. THE INITIAL STATE

I am now in a position to calculate the initial fields before any perturbation is made to the system. It has already been assumed that the velocities in the two layers are constant and have components $\pm\frac{1}{2}$ in the x-direction only. In the equations of motion (2.11) and (2.12), most terms are zero and the following relations are obtained:

$$-\frac{1}{2\epsilon} = -\frac{1}{(1+\sigma/2)}\frac{\partial p_1}{\partial y}$$

$$\frac{1}{2\epsilon} = -\frac{1}{(1-\sigma/2)}\frac{\partial p_2}{\partial y} \qquad (3.1)$$

while differentiating the pressure equation (2.13) yields

$$\frac{\partial (p_1 - p_2)}{\partial y} = R\frac{\partial h}{\partial y} - T\frac{\partial^3 h}{\partial y^3} \qquad (3.2)$$

Note that I am assuming no variation of the initial state of the x-direction. Elimination of the pressures between (3.1) and (3.2) yields an equation for the background variation of height:-

$$\frac{\partial^3 h}{\partial y^3} = \frac{R}{T}\left(\frac{\partial h}{\partial y} - \frac{1}{\epsilon R}\right) \qquad (3.3)$$

which has solutions of the form

$$\frac{\partial h}{\partial y} - \frac{1}{\epsilon R} = A e^{(R/T)^{1/2} y} + B e^{-(R/T)^{1/2} y} \qquad (3.4)$$

The terms on the right-hand side of this equation describe the meniscus which will form at the boundaries at $y = \pm \frac{1}{2}$, the constants A and B being determined by consideration of the angle of contact at the sidewalls. The length scale of the meniscus is $(T/R)^{\frac{1}{2}}$; for values of the parameters which will be of interest this length is small compared to the channel width, and so throughout the bulk of the fluid:

$$\frac{\partial h}{\partial y} = \frac{1}{\epsilon R} \qquad (3.5)$$

This result occurs in the theory of fronts ("Margule's formula") and indicates that away from the boundaries the interface has constant slope. It will be noted that when $\epsilon R < 1$, the interface intersects the upper and lower boundaries rather than the sidewalls. I shall not discuss this case (which is similar to that described in Orlanski 1968) in the present paper. Furthermore, it will prove convenient to assume that the variation of interface height across the channel is small, which leads to the restriction on the range of parameters appropriate to the theory:

$$\epsilon R \gg 1 \tag{3.6}$$

In fact the case $\epsilon R < 1$ cannot be attained for various reasons in the experiments (not least because contact of the lower fluid with the upper surface dissolves the adhesives used!)

To summarize, the basic state is characterized by:

$$\left.\begin{aligned} u_1 &= -1/2 \quad , \quad u_2 = 1/2 \\ v_1 &= 0 \quad , \quad v_2 = 0 \\ h &= h_0 + y/(\epsilon R) \end{aligned}\right\} \tag{3.7}$$

where h_0 is the mean height of the interface.

4. THE PERTURBATION EQUATIONS

I shall now describe a linearized perturbation analysis of the equations (2.9) to (2.13) about the initial state defined by equations (3.7). Define the perturbations as follows:

$$\left.\begin{aligned} u_j &= \pm 1/2 + u_j' \\ v_j &= v_j' \\ h &= h_0 + y/(\epsilon R) + h' \\ p_j &= \bar{p}_j + p_j' \end{aligned}\right\} \tag{4.1}$$

Then, rejecting terms of second or higher order in the perturbed variables, the equations of continuity are:

$$\left.\begin{aligned} \frac{\partial h'}{\partial t} - \frac{1}{2}\frac{\partial h'}{\partial x} &= -\left(h_0 + \frac{y}{\epsilon R}\right)\frac{\partial u_1'}{\partial x} - \frac{v_1'}{\epsilon R} - \left(h_0 + \frac{y}{\epsilon R}\right)\frac{\partial v_1'}{\partial y} \\ \frac{\partial h'}{\partial t} + \frac{1}{2}\frac{\partial h'}{\partial y} &= \left(1 - h_0 - \frac{y}{\epsilon R}\right)\frac{\partial u_2'}{\partial x} - \frac{v_2'}{\epsilon R} + \left(1 - h_0 - \frac{y}{\epsilon R}\right)\frac{\partial v_2'}{\partial y} \end{aligned}\right\} \quad (4.2)$$

At this stage I shall neglect the y-variation in the coefficients of perturbed quantities, obtaining

$$\left.\begin{aligned} \frac{\partial h'}{\partial t} - \frac{1}{2}\frac{\partial h'}{\partial x} &= -h_0\frac{\partial u_1'}{\partial x} - \frac{v_1'}{\epsilon R} - h_0\frac{\partial v_1'}{\partial y} \\ \frac{\partial h'}{\partial t} + \frac{1}{2}\frac{\partial h'}{\partial y} &= (1 - h_0)\frac{\partial u_2'}{\partial x} - \frac{v_2'}{\epsilon R} + (1 - h_0)\frac{\partial v_2'}{\partial y} \end{aligned}\right\} \quad (4.3)$$

The equations of motion are:

$$\left.\begin{aligned} \frac{\partial u_j'}{\partial t} \pm \frac{1}{2}\frac{\partial u_j'}{\partial x} - \frac{1}{\epsilon}v_j' &= -\frac{\bar{\rho}}{\rho_j}p_j' \\ \frac{\partial v_j'}{\partial t} \pm \frac{1}{2}\frac{\partial v_j'}{\partial x} + \frac{1}{\epsilon}u_j' &= -\frac{\bar{\rho}}{\rho_j}p_j' \end{aligned}\right\} \quad (4.4)$$

and the pressure equation is

$$p_1 - p_2 = Rh' - T\left(\frac{\partial^2 h'}{\partial x^2} + \frac{\partial^2 h'}{\partial y^2}\right) \quad (4.5)$$

If I now assume that the perturbations all vary like exp $[i(\omega t + kx)]$, then the equations may be written in the form:

$$i(\omega - k/2)h' = -ikh_0 u_1' - \frac{v_1'}{\epsilon R} - h_0 \frac{\partial v_1'}{\partial y} \tag{4.6}$$

$$i(\omega + k/2)h' = ik(1-h_0)u_2' - \frac{v_2'}{\epsilon R} + (1-h_0)\frac{\partial v_2'}{\partial y} \tag{4.7}$$

$$i(\omega \pm k/2)u_j' - v_j'/\epsilon = -\frac{ik\bar{\rho}}{\rho_j} p_j' \tag{4.8}$$

$$\frac{u_j'}{\epsilon} + i(\omega \pm k/2)v_j' = -\frac{\bar{\rho}}{\rho_j}\frac{\partial p_j'}{\partial y} \tag{4.9}$$

$$p_1' - p_2' = (R + k^2 T)h' - T\frac{\partial^2 h'}{\partial y^2} \tag{4.10}$$

In what follows, I shall generally assume that $h_o = \frac{1}{2}$. This requirement merely reduces the length of expressions and may be trivially relaxed.

5. THE NON-ROTATING CASE

I preface the detailed discussion of the general case by a consideration of the non rotating case. This is somewhat more tractable and illustrates many of the principles applying to the rotating case.

In the absence of rotation, $\epsilon^{-1} = 0$, and so the equations of motion, (4.8) and (4.9) reduce to

$$(\omega \pm k/2)u_j' = -\frac{k\bar{\rho}}{\rho_j} p_j' \tag{5.1}$$

$$i(\omega \pm k/2)v_j' = -\frac{\bar{\rho}}{\rho_j}\frac{\partial p_j'}{\partial y} \tag{5.2}$$

Now the boundary conditions at the sidewalls, $y = \pm\frac{1}{2}$, are simply $v_j = 0$, or, from (5.2)

$$\frac{\partial p_j'}{\partial y} = 0 \tag{5.3}$$

Evidently, this is satisfied provided that p_j' varies like $\sin(\ell y)$, $\ell = 0, \pi, 2\pi$, etc. Consequently,

$$i(\omega \pm k/2)\frac{\partial v_j'}{\partial y} = \frac{\bar{p}}{\rho_j}\ell^2 p_j' \tag{5.4}$$

and so u_j', v_j' can be eliminated from (4.6) and (4.7), yielding

$$\begin{aligned} 2(1+\sigma/2)(\omega - k/2)^2 h' - (k^2+\ell^2)p_1' &= 0 \\ 2(1-\sigma/2)(\omega + k/2)^2 h' + (k^2+\ell^2)p_2' &= 0 \end{aligned} \tag{5.5}$$

From equation (4.10), h' must vary in the same way as p_1', p_2' and so

$$\left(R + [k^2+\ell^2]T\right)h' - p_1' + p_2' = 0 \tag{5.6}$$

Equations (5.5) and (5.6) can be simultaneously satisfied if the determinant

$$\begin{vmatrix} 2(1+\sigma/2)(\omega - k/2)^2 & -(k^2+\ell^2) & 0 \\ 2(1-\sigma/2)(\omega+k/2)^2 & 0 & (k^2+\ell^2) \\ R + (k^2+\ell^2)T & -1 & 1 \end{vmatrix} = 0 \tag{5.7}$$

which after some rearrangement yields a dispersion relation for ω:

$$\omega^2 - \frac{k\sigma}{2}\omega + \frac{1}{4}\left(k^2 - (R + [k^2+\ell^2]T)(k^2+\ell^2)\right) = 0 \qquad (5.8)$$

and so

$$\omega = \frac{k\sigma}{4} \pm \frac{1}{2}\left[\frac{k^2\sigma^2}{4} - k^2 + (R+[k^2+\ell^2]T)(k^2+\ell^2)\right] \qquad (5.9)$$

For instability, I require ω to be complex, a situation which attains when

$$(1 - \sigma^2/4)k^2 > (k^2+\ell^2)(R + [k^2+\ell^2]T) \qquad (5.10)$$

Certain important points emerge:-

(1) Instability is promoted by small R

(2) Surface tension (as measured by T) is a stabilizing mechanism

(3) The meridonal wavenumber, ℓ, has always a stabilizing effect; consequently the most unstable waves have $\ell = 0$.

(4) Finite σ has a weakly stabilizing effect; but it will be observed that the main effect of non-zero σ is to introduce a slow drift of the unstable waves, which have a phase speed $\sigma/4$. Note that σ is always less than 1 by definition, and will generally be small (about 10^{-2} in the experiments).

It follows that in the most unstable case (ie, $\sigma = 0$, $\ell = 0$ and $T = 0$) that the inequality (5.10) reduces to $k^2 > Rk^2$, and so <u>a necessary condition for instability is $R < 1$</u>. The growth rate q (which is $-\gamma_m(\omega)$) is

$$q = \frac{k}{2}(1-R)^{1/2} \qquad (5.11)$$

which increases indefinitely with k. Such behaviour is clearly unphysical, and at large k some other physical mechanism must stabilize the waves.

One such mechanism is provided by the surface tension, since the term in T also involves the wavenumber. In general q is given by

$$q^2 = -Tk^4 + (1-R-\sigma^2/4 - 2l^2T)k^2 - l^2(R+l^2T) \qquad (5.12)$$

It therefore has a maximum value when

$$k^2 = \frac{(1-R-\sigma^2/4)}{2T} - l^2 = k_{max}^2 \qquad (5.13)$$

and falls to zero when

$$k^2 = k_{max}^2 \pm \left[\frac{(1-R)^2}{4T^2} - \frac{l^2}{T} - \frac{\sigma^2 k_{max}^2}{4T} \right]^{1/2} \qquad (5.14)$$

Figure (2) shows q as a function of k for various R. Both σ and T have values of 10^{-2}, which is typical of the experiments, and l is taken as zero. Note the nearly linear dependence of q on l for small k, and the rather sharp short wave cut-off when surface tension is effective. As $R \rightarrow 0$, the curves tend to an asymtotic form.

6. ROTATING CASE – DERIVATION OF DISPERSION RELATION

In the general case when rotation may not be neglected, equations (4.9) and (4.10) may be rearranged to give:

$$u_j' = \frac{\bar{\rho}\,[(\omega \pm k/2)k p_j' - 1/\epsilon\ \partial p_j'/\partial y]}{\rho_j\,[1/\epsilon^2 - (\omega \pm k/2)^2]} \qquad (6.1)$$

$$v_j' = \frac{i\,\bar{\rho}\,[k/\epsilon\ p_j' - (\omega \pm k/2)\partial p_j'/\partial y]}{\rho_j\,[1/\epsilon^2 - (\omega \pm k/2)^2]} \qquad (6.2)$$

The basic boundary condition is still $v_j = 0$, $y = \pm \frac{1}{2}$, but this now implies a more complicated boundary condition on the pressure:

$$(\omega \pm k/2)\frac{\partial p_j'}{\partial y} - \frac{k}{\epsilon} p_j' = 0, \quad \ell = \pm 1/2 \tag{6.3}$$

This equation may be satisfied if

$$p_j' = p_j^0 \left(\cos(\ell y) + \alpha_j \sin(\ell y) \right) \tag{6.4}$$

where $\ell = 0, \pi, 2\pi$ etc; when $\ell = \pm\frac{1}{2}$ this form satisfies the boundary conditions provided that

$$\alpha_j = -(\omega \pm k/2)\ell\epsilon/k \tag{6.5}$$

α_j is a measure of the geostrophy of the flow, indicating the degree to which flow is not parallel to the isobars. As $\epsilon \to 0$, it will be observed that pressure variations co-incide with the variations of v, which is the usual geostrophic case.

The y-variation of the heights must be expressed in a similar way, ie $h' = h_0'$ (cos ly + Γ sin ly). Substitution into the pressure equation, equation (4.10) would enable the constant Γ to be determined. However, it is not necessary to do this, as will be seen.

Equations (6.1) and (6.2) are used to eliminate the velocities from the height equations:

$$(1+\sigma/2)\left[\frac{1}{\epsilon^2} - (\omega - \tfrac{k}{2})^2\right]h' = -\frac{k^2}{2}p_1' - \frac{k p_1'}{\epsilon^2 R(\omega - k/2)} + \frac{1}{\epsilon R}\frac{\partial p_1'}{\partial y} + \frac{1}{2}\frac{\partial^2 p_1'}{\partial y^2}$$

$$(1-\sigma/2)\left[\frac{1}{\epsilon^2} - (\omega + \tfrac{k}{2})^2\right]h' = \frac{k^2 p_2'}{2} - \frac{k p_2'}{\epsilon^2 R(\omega + k/2)} + \frac{1}{\epsilon R}\frac{\partial p_2'}{\partial y} - \frac{1}{2}\frac{\partial^2 p_2'}{\partial y^2} \tag{6.6}$$

I then substitute the y-variation of h' and p_j' and equate coefficients of cos (ly) to obtain:

$$(1+\sigma/2)\left[\frac{1}{\epsilon^2}-(\omega-\frac{k}{2})^2\right]h' + \left[\frac{1}{2}(k^2+\ell^2)+\frac{2k}{\epsilon^2 R(\omega-k/2)}\right]p_1' = 0$$

$$(1-\sigma/2)\left[\frac{1}{\epsilon^2}-(\omega+\frac{k}{2})^2\right]h' - \left[\frac{1}{2}(k^2+\ell^2)-\frac{2k}{\epsilon^2 R(\omega+k/2)}\right]p_2' = 0 \qquad (6.7)$$

A similar substitution in the pressure equation (4.10) yields

$$\left(R+[k^2+\ell^2]T\right)h' - p_1' + p_2' = 0 \qquad (6.8)$$

Note at this stage that the same set of equations would have been obtained by equating the sine coefficients in the equations (6.6) and (4.10).

Proceeding just as before, for equations (6.7) and (6.8) to be simultaneously satisfied, their determinant must be zero. After considerable manipulation, this condition leads to the polynomial dispersion relation for ω:

$$\sum_{i=0}^{4} a_i \omega^i = 0 \qquad (6.9)$$

where

$$a_0 = k^2\left[(k^2+\ell^2)(R+[k^2+\ell^2]T)\left(\frac{2}{\epsilon^2 R(k^2+\ell^2)}-\frac{1}{4}\right)^2-\left(\frac{1}{\epsilon^2}-\frac{k^2}{4}\right)\left(\frac{2}{\epsilon^2 R(k^2+\ell^2)}-\frac{1}{4}\right)\right]$$

$$a_1 = -\sigma k\left[\frac{2}{\epsilon^2 R(k^2+\ell^2)}\left(\frac{1}{\epsilon^2}-\frac{k^2}{4}\right)-k^2\left(\frac{1}{\epsilon^2 R(k^2+\ell^2)}-\frac{1}{8}\right)\right]$$

$$a_2 = 2k^2\left(\frac{3}{\epsilon^2 R(k^2+\ell^2)}-\frac{1}{8}\right)-\left(\frac{1}{\epsilon^2}-\frac{k^2}{4}\right)-\frac{(k^2+\ell^2)(R+[k^2+\ell^2]T)}{4} \qquad (6.10)$$

$$a_3 = -\sigma k\left(\frac{2}{\epsilon^2 R(k^2+\ell^2)}+\frac{1}{2}\right)$$

$$a_4 = 1$$

The roots of this equation are not readily obtained by analytic means, and a numerical method has been employed to survey the behaviour of the roots in the (ϵ, R, T, σ) parameter space. The numerical scheme is outlined in the Appendix, and the results are described in subsequent sections. However, the following principal results are again obtained:

(a) Increasing l invariably stabilizes the system, as in the non-rotating case.

(b) σ is an unimportant variable and only makes slight differences to the form of the roots.

(c) When R is large (ie, when R > 10 or so) the effects of surface tension are slight.

These observations enable the dispersion relation to be somewhat simplified. First, setting $\sigma = 0$ and $l = 0$ yields:

$$\omega^4 + \left(\frac{6}{\epsilon^2 R} - \frac{1}{\epsilon^2} - \frac{k^2}{4}(R + k^2 T)\right)\omega^2 + \left(\frac{2}{\epsilon^2 R} - \frac{k^2}{4}\right)\left[(R+k^2T)\left(\frac{2}{\epsilon^2 R} - \frac{k^2}{4}\right) - \frac{1}{\epsilon^2} + \frac{k^2}{4}\right] \quad (6.11)$$

This simplifies further when $T \longrightarrow 0$ to

$$\omega^4 + \left(\frac{6}{\epsilon^2 R} - \frac{1}{\epsilon^2} - \frac{k^2 R}{4}\right)\omega^2 + \left(\frac{2}{\epsilon^2 R} - \frac{k^2}{4}\right)\left(\frac{1}{\epsilon^2} - \frac{k^4}{4}[R-1]\right) \quad (6.12)$$

Even this final simplified form is not easily factorized without further approximation; consequently most of the results will be based on numerical solutions to equations (6.10) and (6.11).

There are but three possibilities for the roots of the simplified dispersion relationships (6.11) and (6.12):

(a) Both roots for ω^2 may be real and positive, implying real pairs of values of ω of opposite sign. This describes pairs of travelling waves on propagating in opposite directions.

(b) One or both roots of ω^2 may be negative. Thus pairs of imaginary values of ω are found, which correspond to stationary waves, one growing and one decaying.

(c) The roots may be complex, in the form of complex conjugates. Consequently ω must be of the general form $\pm(\alpha + i\beta)$. Physically this implies pairs of travelling, amplifying or decaying waves, propagating in opposite directions. The somewhat unhappy term "over stability" is sometimes applied to this situation.

It will be noted that whenever cases (b) or (c) apply, there must be at least one unstable wave mode.

7. SHORT WAVE INSTABILITIES

In comparing these calculations with laboratory experiments, the effects of the boundedness of the system in the x-direction should be taken into account. The simplest, and most realistic, case is to assume periodicity in the x-direction. As a result the spectrum of admissible waves is discrete and has a minimum wavenumber defined by the length of the channel.

In this section it seems sensible to describe the roots of equation (6.9) when a rather coarse resolution in k-space, corresponding to a channel not much longer than it is wide, is employed. Various rather weak, long wave instabilities will be discussed in section 8.

Equation (6.9) was solved for a large number of suitably chosen points on the ($\mathcal{E}$, R) plane, with $\sigma = 10^{-2}$ and $T = 10^{-2}$, which is typical of the experiments. For each ($\mathcal{E}$, R), the roots were found for values of k ranging from .1 upwards in steps of .1 (ie, the channel had length 10L). By examination of the resulting roots the growth rate and wavenumber of the most unstable wave could be determined.

Figure (3) shows the growth rate of instabilities on the (ϵ, R) plane. The dotted lines delineate the region where the interface slope becomes too steep to apply the theory usefully. Two areas of major instability are noted: first, a fast instability when $R < 1$, which corresponds to the Kelvin-Helmholtz instability when the rotation is negligible, and second, a slower instability when $\epsilon^2 R < 50$ or so. Between these two regions lies an area of slower long wavelength instability which will be discussed more fully in section 7.

The Kelvin-Helmholtz instability is but little affected by rotation, down to the Rossby number at which the theory breaks down. Figure (4) shows a series of curves of growth rate, versus wavenumber for R = 0.95 and various Rossby numbers. As the rotation increases, the longest waves become more unstable, while the maximum growth rate increases slightly. The shortwave cut off, and wavenumber for maximum growth rate are relatively unaffected. Broadly however, this instability is adequately described by the non-rotating theory of section (5).

The instability at large R and smaller ϵ corresponds to the baroclinic instability described by quasi-geostrophic theory. The growth rate curves show both a short wave and long wave cut off, with a maximum growth rate between, and it will be noted that the maximum growth rate, and the wavenumber of maximum growth rate are almost exactly functions of the single parameter $\epsilon^2 R$. It will be observed that

$$\epsilon^2 R = \frac{(\Delta\rho/\bar{\rho})\, g D}{4\Omega^2 L^2} \qquad (7.1)$$

which is the analogue of the parameter Θ (see, for example Hide & Mason 1975), used to describe baroclinic instability in a thermally driven annulus. Figure (5) shows growth rate curves for the baroclinic instability for various values of $\epsilon^2 R$.

Although the dispersion relations (6.11) or (6.12) have not been solved analytically certain results pertinant to the baroclinic instability are readily obtained. The baroclinic instability occurs at large Richardson number, and consequently the effect of surface tension in the pressure equation is negligible. The dispersion relation (6.12) is therefore appropriate. When the constant term in this equation is negative, the ω^2 must be real, and one root must be negative, corresponding to imaginary ω and an unstable disturbance. This condition reduces to

$$\frac{4}{\epsilon^2(R-1)} < k^2 < \frac{8}{\epsilon^2 R} \tag{7.2}$$

or, for large R

$$2\,(\epsilon^2 R)^{-1/2} < k < 2\sqrt{2}\,(\epsilon^2 R)^{-1/2} \tag{7.3}$$

This is in excellent agreement with the numerically determined long and short wave cut offs, as exemplified by Figure (5). Furthermore, the results of many numerical solutions of the dispersion relation at large R shows that

$$\begin{aligned} q_{max} &= 3.16\,(\epsilon^2 R)^{-1/2} \\ k_{max} &= 2.40\,(\epsilon^2 R)^{-1/2} \end{aligned} \tag{7.4}$$

Note that k_{max} lies ~~about~~ almost exactly half way between the long and short wave cut offs.

For R $\sim$ 1, the long and short wave cut offs given by equation (7.2) coincide when R = 2. This appears to define an effective limit for the baroclinic instability. For R $<$ 2 certain instabilities are possible, which are more appropriately discussed in the next section.

8. LONGWAVE INSTABILITIES

When $R < 18$ and for relatively rapid rotation (say $\epsilon < 20$), new classes of instabilities become important. They are characterized by having maximum growth rates as $k \to 0$, and so will be termed "longwave instabilities".

Once more, I will restrict attention to the simplified dispersion relation (6.11). This yields complex roots for ω^2 when its determinant is negative; after some algebraic manipulation, the discriminant is found to be:

$$\mathcal{D} = (R-2)\left[\frac{(R-18)}{\epsilon^4 R} + \frac{k^4(R-2)}{16} + \frac{k^2(R+2)}{2\epsilon^2 R} \right] \tag{8.1}$$

When $R > 18$, D must be positive and only real values of ω^2 are possible. However for $2 < R < 18$, D is always negative for sufficiently small k, and takes its most negative value when $k \to 0$. I conclude that there must be long wave over stability when $2 < R < 18$. The baroclinic instability discussed in section (7) still occurs for larger k, but in some regions of parameter space the long-wave overstability has the larger growth rate.

When $1 < R < 2$, the case is reversed; D is positive for small k and takes on its most positive value as $k \to 0$. The most negative value of ω^2 is

$$\omega^2 = -\frac{1}{2}\left(\frac{6}{\epsilon^2 R} - \frac{1}{\epsilon^2} - \frac{k^2 R}{4} + \mathcal{D}^{1/2} \right) \tag{8.2}$$

When $k \to 0$, $\mathcal{D}^{\frac{1}{2}}$ can be approximated using the binomial theorem to yield

$$\mathcal{D}^{1/2} \doteq \frac{1}{\epsilon^2}\left[\frac{(2-R)(18-R)}{R}\right]^{1/2}\left[1 - \frac{(R+2)}{4(18-R)}\epsilon^2 k^2\right] \tag{8.3}$$

Consequently, it is evident that when k is small, ω^2 has a negative root which has an extreme value at $k \to 0$, thus implying a long wave instability.

A further complication will be noted when k is not small, for if the expression for D is rewritten as:

$$D = (2-R)\left[\frac{(18-R)}{\epsilon^4 R} - \frac{k^2(R+2)}{2\epsilon^2 R} + \frac{(R-2)k^4}{16}\right] \tag{8.4}$$

it is evident that D is positive when k is either very small or very large; at intermediate values, however, there remains the possibility that D may be negative, giving overstability. Writing the term in square brackets in equation (8.4) as a quadratic in k^2, the condition for overstability is:-

$$k^4 - \frac{8(R+2)}{\epsilon^2 R(2-R)}k^2 + \frac{16(18-R)}{\epsilon^4 R(2-R)} < 0 \tag{8.5}$$

which is satisfied when

$$\frac{4(R+2)}{\epsilon^2 R(2-R)} - d^{\frac{1}{2}} < k^2 < \frac{4(R+2)}{\epsilon^2 R(2-R)} + d^{\frac{1}{2}} \tag{8.6}$$

It can be shown that

$$d^{\frac{1}{2}} = \frac{4(R+2)}{\epsilon^2 R(2-R)}\left[1 - \frac{R(18-R)(2-R)}{(R+2)^3}\right]^{\frac{1}{2}} \tag{8.7}$$

This is real provided $R > 1.505$, and leads to positive limits on k^2 when $1.505 < R < 2$. In this range therefore, there is instability of long waves and overstability for a range of somewhat shorter waves. The variation of the region of overstability with R is shown in Figure (6). In all cases which have been considered, however, the overstability is considerably weaker than the long wave instability; it would only be important for a channel of such a length as to exclude the more unstable long waves.

When $R < 1$, the long wave instability persists, but at shorter wavelengths the faster Kelvin-Helmholtz mode generally dominates. Over all the feasible region of the (ϵ, R) plane, the long wave instability is comparable to the Kelvin-Helmholtz instability only as $R \to 1$.

The series of figures (7), (8) and (9) demonstrate the various transitions in the longwave instability as R is increased. The instability curves are for $\epsilon = 5$, $T = 10^{-2}$, $\sigma = 0$, and $l = 0$. Note that it has been necessary to employ different scales for the various figures, and care should be exercised in comparing them.

Figure (7) shows curves of q versus k for $R < 1$. Longwave instability is a pronounced feature of all the curves, while above $k \sim 1$ the characteristic Kelvin-Helmholtz instability curve is observed (cf figure 2). The Helvin-Helmholtz instability is more important when $R = 0.8$, but the long wave instability dominates when $R = 0.9$. As R increases further, the Kelvin-Helmholtz curve becomes entirely subsidiary.

Two cases in the range $1 < R < 2$ are shown in Figure (8): the curves are for $R = 1.2$ and $R = 1.7$. Both show a region of longwave instability, but a much weaker, shorter wave overstability can be discerned in the latter case.

The stability curves in the range $2 < R < 18$ show less variation. Figure (9) shows some typical examples for $E = 5$. In addition to a region of longwave overstability, the baroclinic wave peak is seen at shorter wavelengths. In some regions of parameter space (not traversed in this scan) the longwave overstability dominates; the height, width and position of the baroclinic peak vary in accordance with equations (7.2), (7.3) and (7.4). As R approaches 18, the long wave overstability region disappears.

These results are summarized in Figure (10) which shows the regions where the various instabilities appear and dominate; the data is obtained from numerical solutions of equation (6.11) with $T = .01$. The limits of the various instabilities are denoted by solid lines, and the regions where they dominate by solid lines

with hatching. The broken lines delimit the regions where the theory is expected to be poorly applicable. Four regions, where Kelvin–Helmholtz instability, long-wave instability, baroclinic instability and longwave overstability respectively dominate may be distinguished. It is interesting that the region of the $\epsilon - R$ plane shown in Figure (10) comprises much of the region which is amenable to experimental investigation.

9. DISCUSSION

Despite its relatively simple appearance, the stability of the two layer system is surprisingly complicated, and waves can grow in a variety of ways. The simple classification of the experimenters, who have described long wavelength disturbances as "baroclinic waves" and short wavelength disturbances as "Kelvin–Helmholtz waves" is certainly an over simplification; at least four distinct varieties of instability can be distinguished:-

(a) Kelvin–Helmholtz instability

(b) Baroclinic instability

(c) Long wave instability

(d) Long wave "overstability" or travelling, amplifying disturbances.

The instabilities (a) and (c), (b) and (d) and (c) and (d) can all co-exist in various points of parameter space; precisely which would dominate in a real situation would depend on the periodicity of the channel. The experimental conjecture that instabilities (a) and (b) may co-exist is not supported, although it is likely that background field provided by a finite amplitude baroclinic wave could be locally unstable to Kelvin–Helmholtz instability. This possibility can be checked by allowing h_o to be other than $\frac{1}{2}$ in the equations (4.6) to (4.10) and repeating the ensuing analysis.

Surface tension effects are only important for the Kelvin–Helmholtz waves. Evidently the maximum growth rates of the various long wave instabilities is unaffected by surface tension (whose effect is proportional to k^2), while the baroclinic instability occurs at larger R so that the surface tension makes

very little contribution to the pressure equation. For the baroclinic instability, it can easily be shown, using equation (7.4), that the condition for the surface tension to contribute more than 10% to the pressure for the most unstable wave is

$$\epsilon^2 > \frac{1}{25T} \qquad (9.1)$$

Thus for the typical value of T of .01, ϵ must exceed 2. Reference to Figures (3) and (10) shows that the baroclinic instability is very weak and uninteresting throughout almost all this region.

The effect of σ finite is again small, although it has not been investigated exhaustively. The most important effect is to make all instabilities travelling waves, although one may still usefully distinguish between rather slowly propagating instabilities whose phase speed depends on σ (corresponding to what I have described as "instabilities") and more quickly propagating instabilities whose phase speed is but weakly dependent on σ (my "overstabilities".) The effects on the transitions and growth rates is minimal, although the growth rates of the longwave overstability in the range $2 < R < 18$ are slightly changed. As ϵ becomes small the value of R at which the longwave overstability is removed is somewhat larger than 18. However these effects are most pronounced in the region where interface slope exceeds .1, and so are not of great interest.

The introduction of slow rotation is however, of crucial importance. The Kelvin-Helmholtz disturbances are made slightly more unstable, but more importantly, the whole range of instabilities for $R < 18$ is permitted. These instabilities can be expected to be of considerable interest in the range of parameters accessible to laboratory experiment.

A number of extensions of this work are of possible interest. It has turned out that the introduction of structure in the y-direction is fairly uninteresting, and that where instability occurs, the $l = 0$ mode is invariably the most important. This suggests that re-casting the analysis to treat possible variations of flow in the z-direction might be more fruitful. Such a procedure would enable the

effects of Ekman layers and topography on the bounding surfaces to be introduced, and is likely to be of greater interest, particularly when the rotation is slow so that the two-dimensionality of the flow in each layer is indefensible.

As far as the instabilities presented here are concerned, the energy sources should be investigated in detail. The various long wave instabilities have growth rates which depend both on R and ϵ, (although the conditions under which they appear depend solely on R), suggesting that they may be related to the baroclinic disturbances at large R.

Finally since the new instabilities have growth rates which tend to a maximum as $k \to 0$, a careful comparison of the linear theory with experiments must take account of the effects of curvature. Consequently there is a case for repeating the analysis for the much more complicated case of annular or cylindrical geometry.

However, a more interesting line of enquiry is likely to be in the direction of finite amplitude disturbances and the effects of non-linearity, and in the direction of non-linear interactions between the various waves which the system supports. Analysis is likely to be heavy, and numerical techniques may have to be employed.

I must thank Dr P J Mason for suggesting this problem to me, Dr H Leach for generously allowing me to make use of material pertaining to the problem, and Mr J King for advice concerning the experiments.

10. BIBLIOGRAPHY

Chandrasekhar, S. (1961): Hydrodynamic and Hydromagnetic Stability (especially Chapter XI). Oxford University Press.

Hart, J E (1972): A laboratory study of baroclinic instability. Geophys. Fluid Dyn. 3 181.

Hart, J E (1973): On the behaviour of large amplitude baroclinic waves. J. Atmos. Sci. 30 1017.

Hart, J E (1976): Modulation of an Unstable Baroclinic Wave Field. J. Atmos. Sci. 33 1874.

Hide, R (1975): Two Layer Model of Baroclinic Instability with Sloping Endwalls. Unpublished manuscript.

Hide, R & Mason, P J (1975): Sloping Convection in a Rotating Fluid. Advances in Physics 24 47.

Lorenz, E N (1963): The Mechanics of Vacillation. J. Atmos. Sci. 20 448.

Orlanski, J (1968): Instability of Frontal Waves. J. Atmos. Sci. 25 178.

Pedlosky, J (1971): Finite Amplitude Baroclinic Waves with Dissipation. J. Atmos. Sci. 28 587.

Pedlosky, J (1972): Limit Cycles and Unstable Baroclinic Waves. J. Atmos. Sci. 29 53.

Williams, B S (1976): The John Hart Experiment: A Laboratory Study of Baroclinic Instability. Met O 21 Sandwich Student Report.

APPENDIX: Numerical Solution of Dispersion Relationships

When the dispersion relationships (6.11) and (6.12) apply the location of the roots for ω is obtained straightforwardly by the solution of quadratic equations. However, when it is required to solve the full dispersion relationship, equation (6.10), approximate methods must be used.

The procedure was as follows. Having calculated the coefficients of the polynomial, a first (generally complex) root is located by the Newton-Raphson iterative technique. Once found, this root is divided out, leaving a cubic equation which is treated in the same way. Finally, reduction to a quadratic enables the remaining two roots to be determined.

The Newton-Raphson procedure can fail to converge onto a root on occasions, and a computer program must take account of this. The difficulty can generally be removed by an initial guess at the root which is sufficiently close to the actual root, and a revised guess frequently assures the convergence of a recalcitrant case. A particular difficulty with equations with real coefficients arises when the search process attempts to cross the real axis; because the polynomial must be symmetric about the real axis the search can become stuck here. In all but a handful of cases, a root was found by taking a second initial guess in the opposite half plane.

All calculations were performed in double precision, as the roots can be very sensitive to small errors in the coefficients.

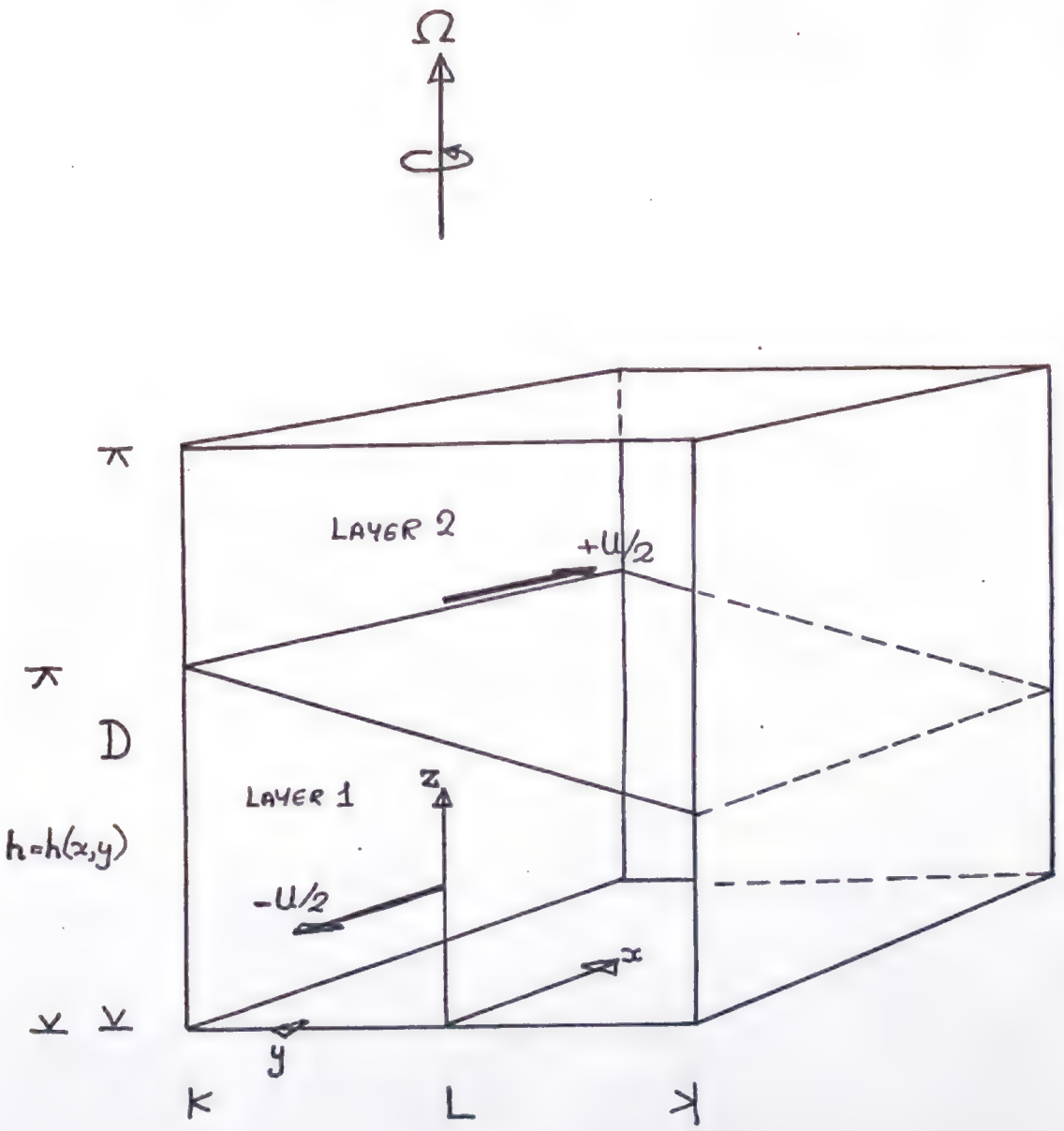

Fig (1): The configuration under discussion.

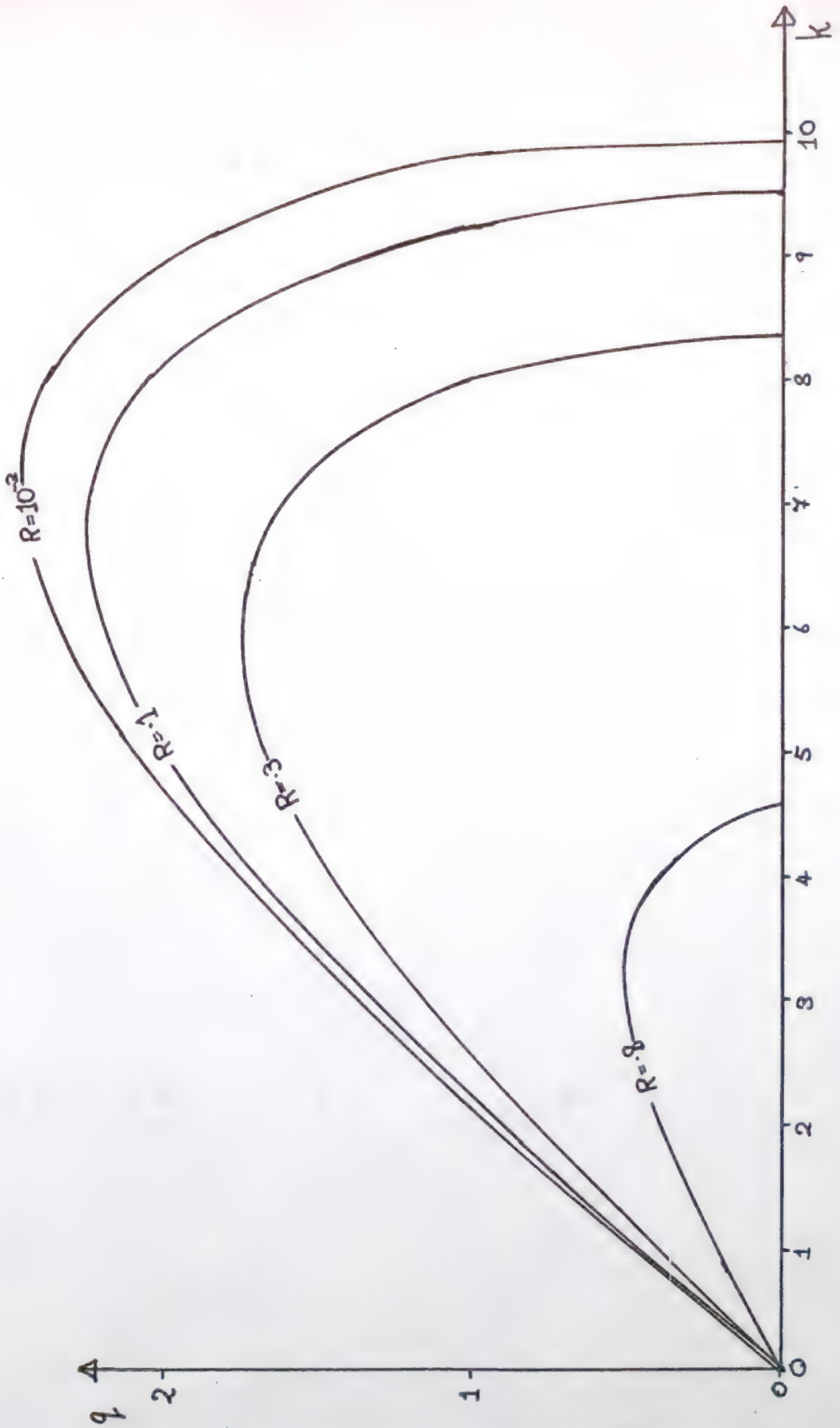

Fig (2): The non-rotating theory of Kelvin-Helmholtz instability.

Curves of growth rate against k are shown for various R and T= 0.01.

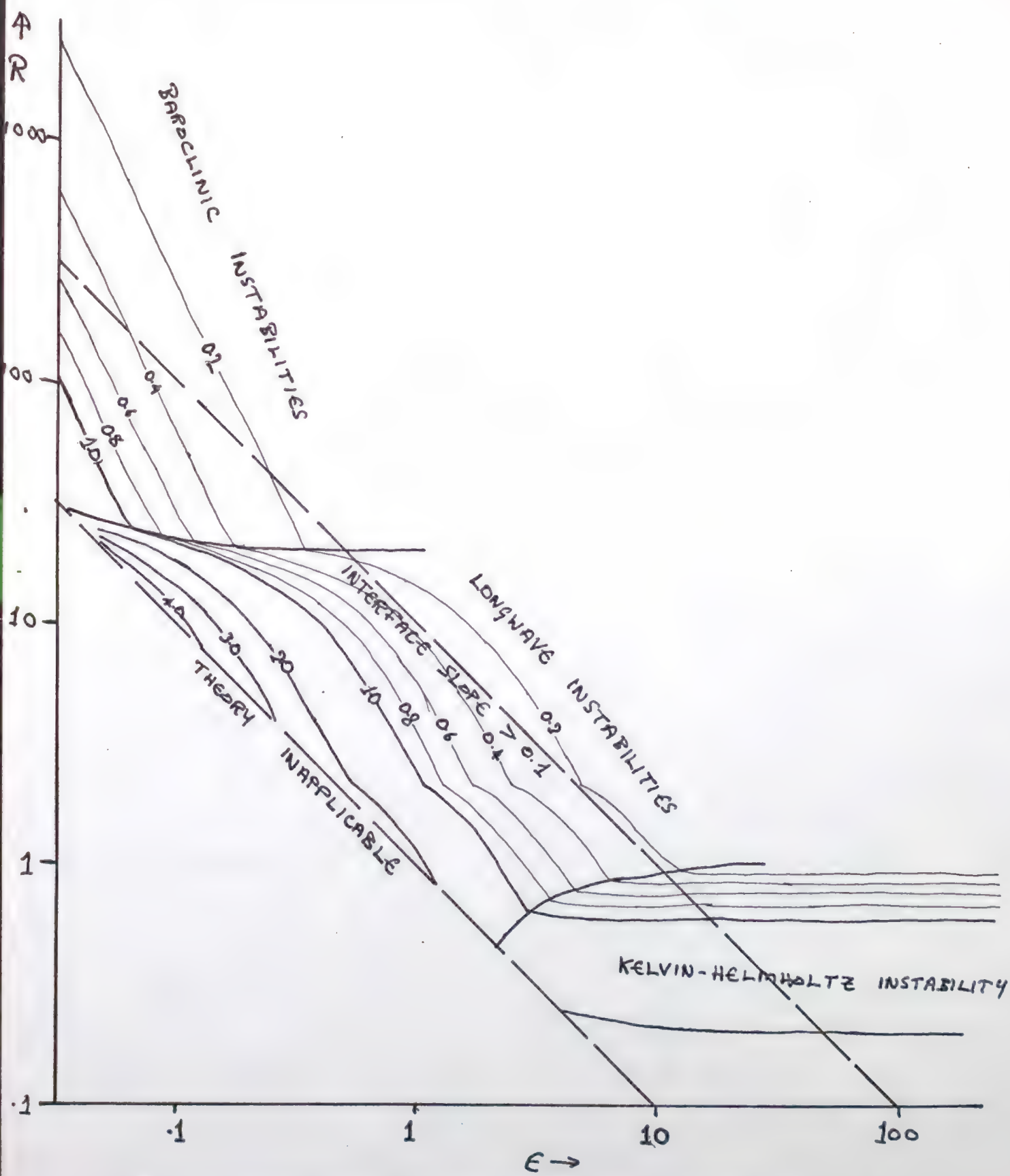

Fig (3): Growth rate of the most unstable wave as a function of ϵ and R. Other parameters are T= 0.01, σ = 0.01 and l=0.

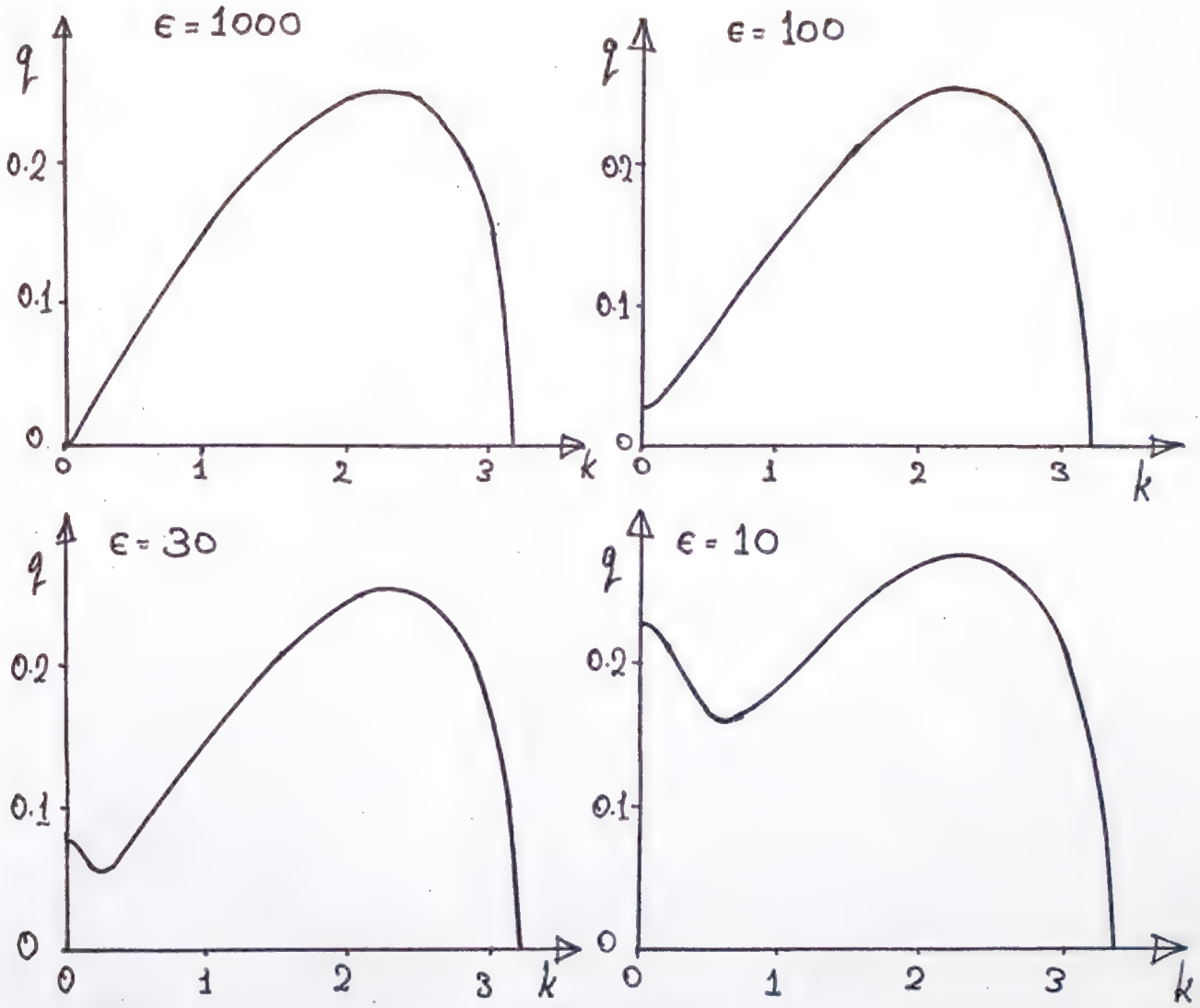

Fig (4): The effect of rotation on the Kelvin-Helmholtz instability. Growth rate curves are shown for R= 0.95, T= 0.01, σ=0, l=0 and various ϵ.

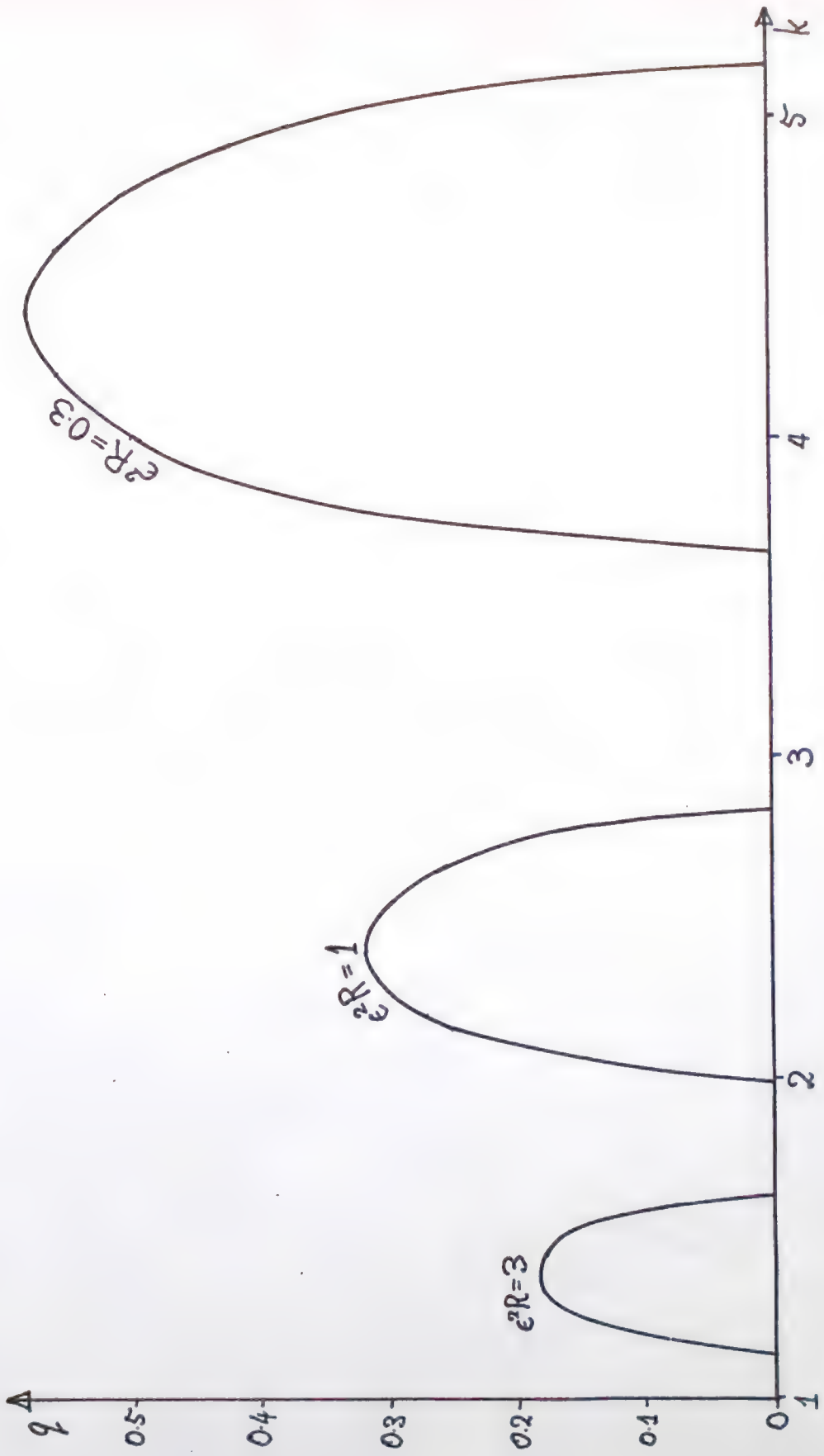

Fig (5): Baroclinic instability curves as a function of the parameter $(\epsilon^2 R)$. In these runs, l=0, T= 0.01 and σ =0 . R exceeded 100 in all cases.

$4(\epsilon^2 R)^{-\frac{1}{2}}\left(\frac{R+2}{R-2}\right)^{\frac{1}{2}} k$

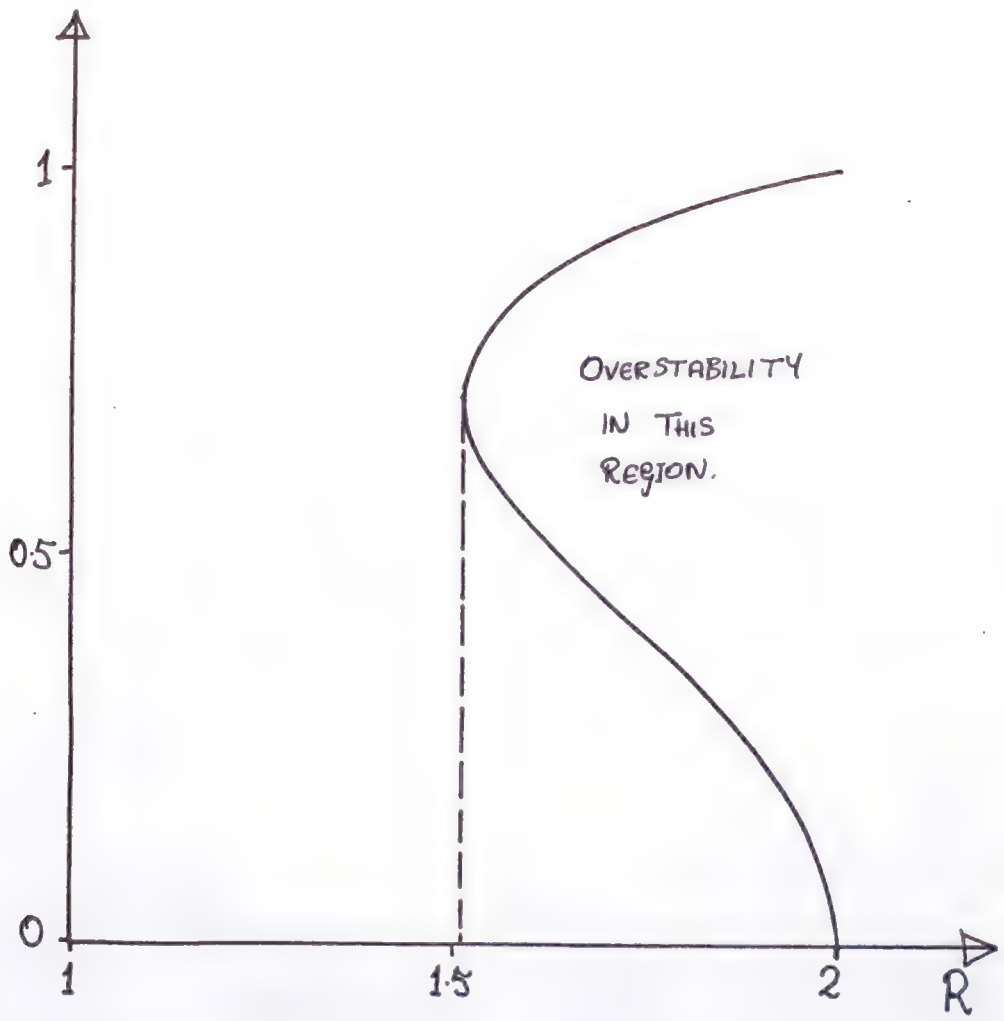

Fig (6): Demonstrating the range of k for which overstability is found when $1 < R < 2$.

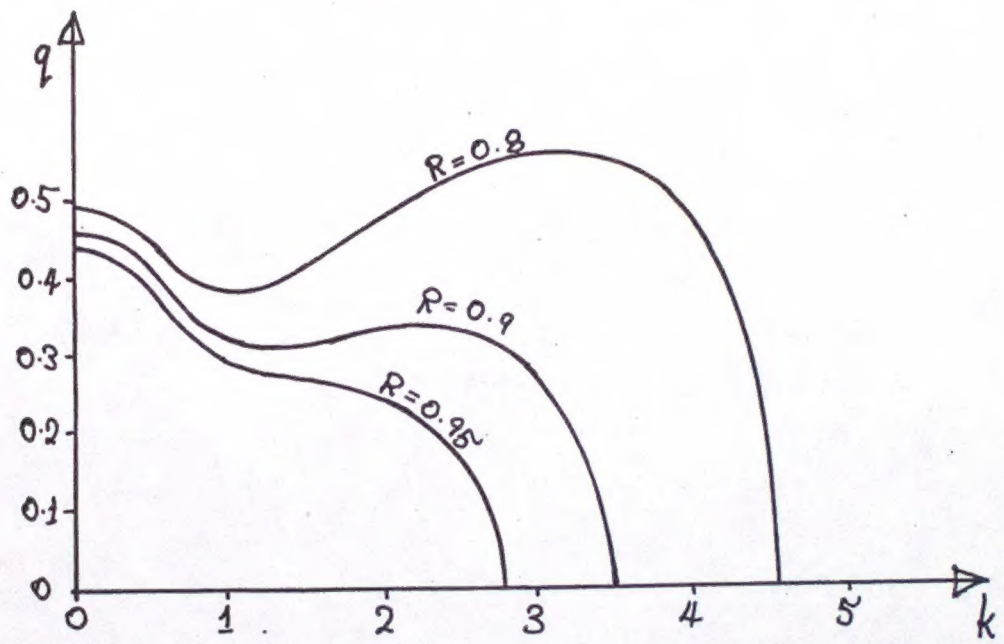

Fig (7): The dependence of Kelvin-Helmholtz instability on R for $\epsilon = 5$. Other parameters are T= 0.01, σ=0 and 1=0.

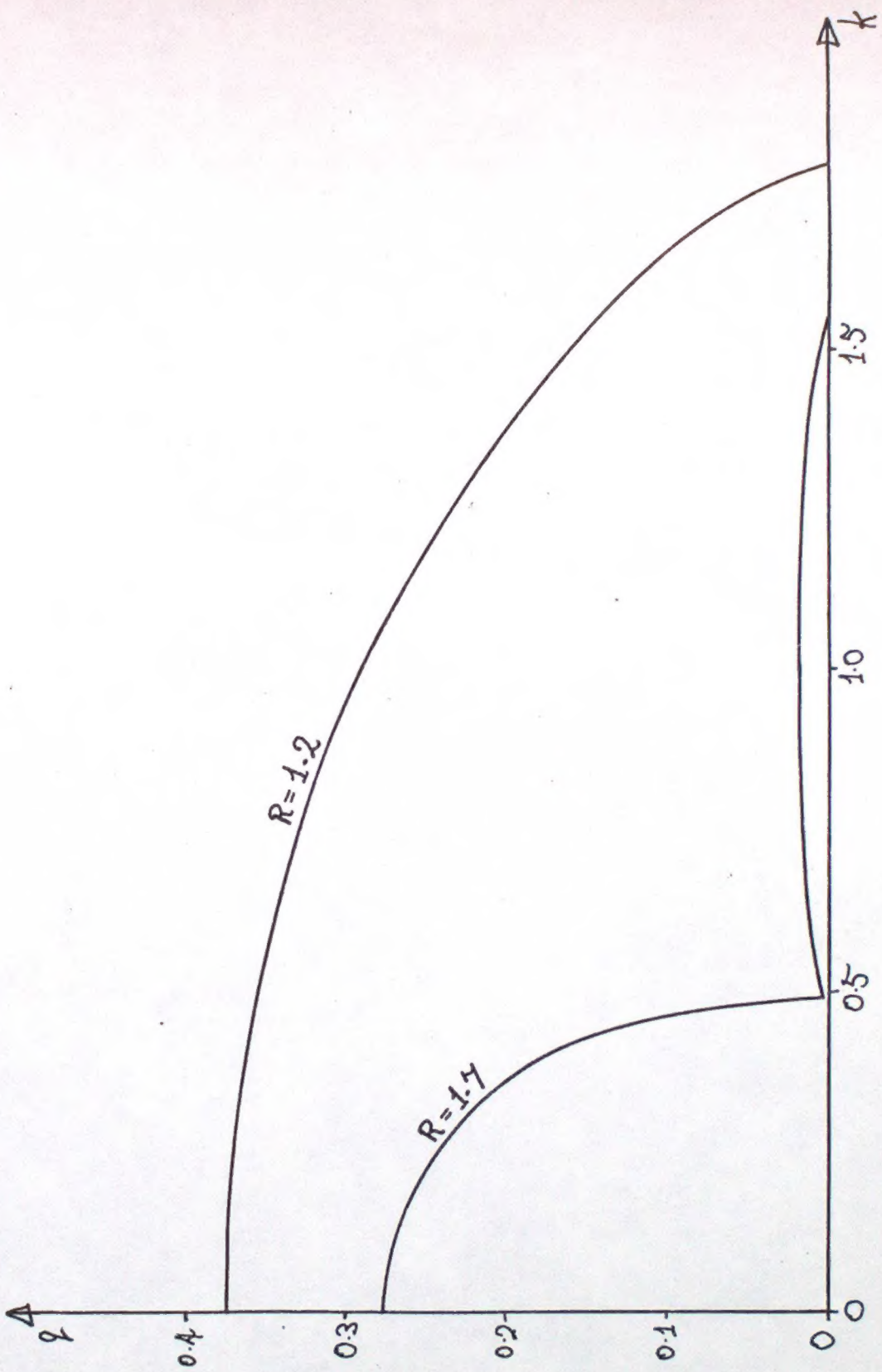

Fig (8): Illustrating the longwave instability in the range $1 < R < 2$. The curve for R=1.7 also shows an area of overstability. Other parameters are $\epsilon = 5$, T=0.01, $\sigma = 0$, and l=0.

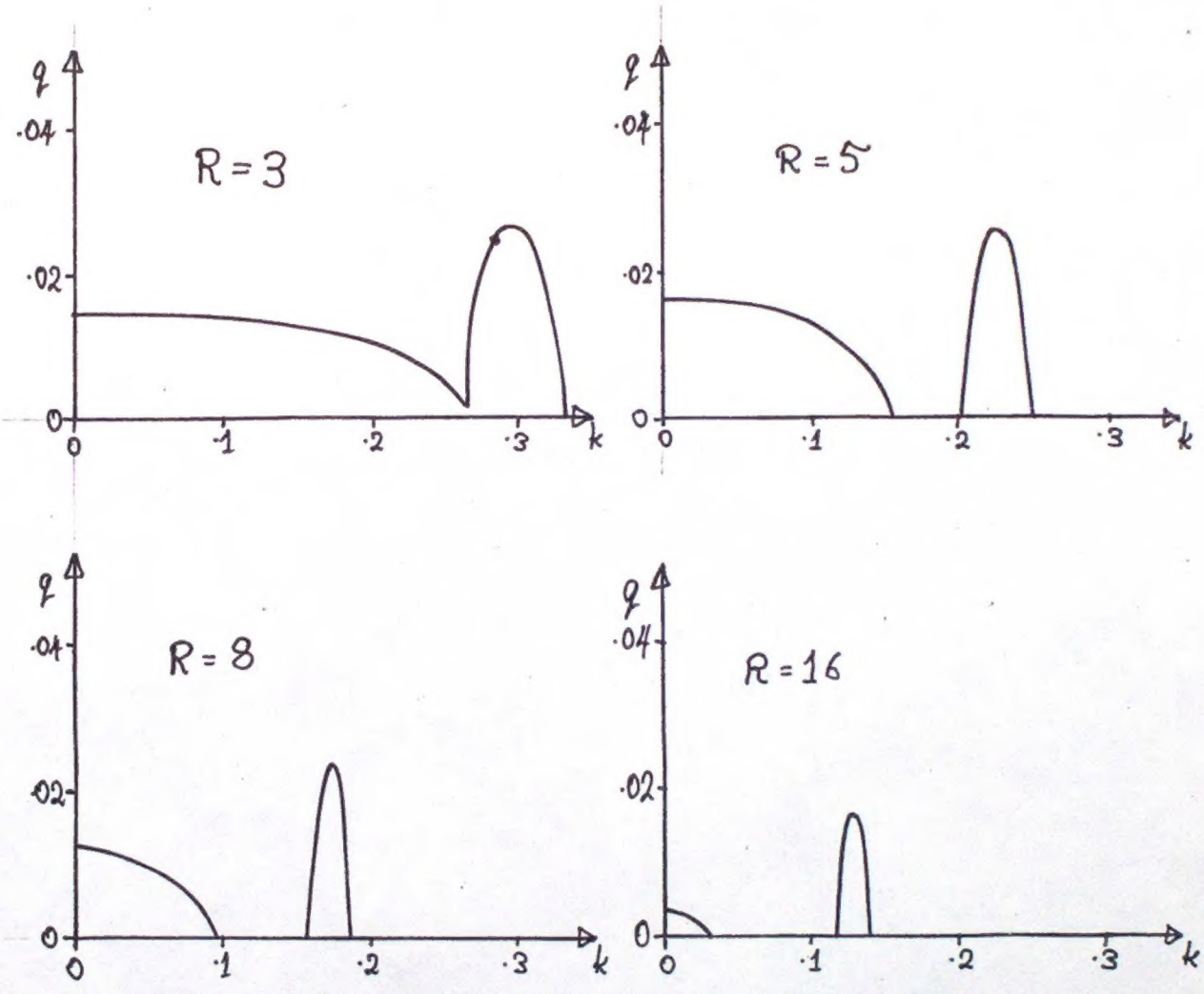

Fig (9): Growth rate curves in the range $2 < R < 18$. Overstability is present at small k, and baroclinic instability at somewhat larger k. Parameters are $\epsilon = 5$, T=0.01, $\sigma = 0$ and l=0.

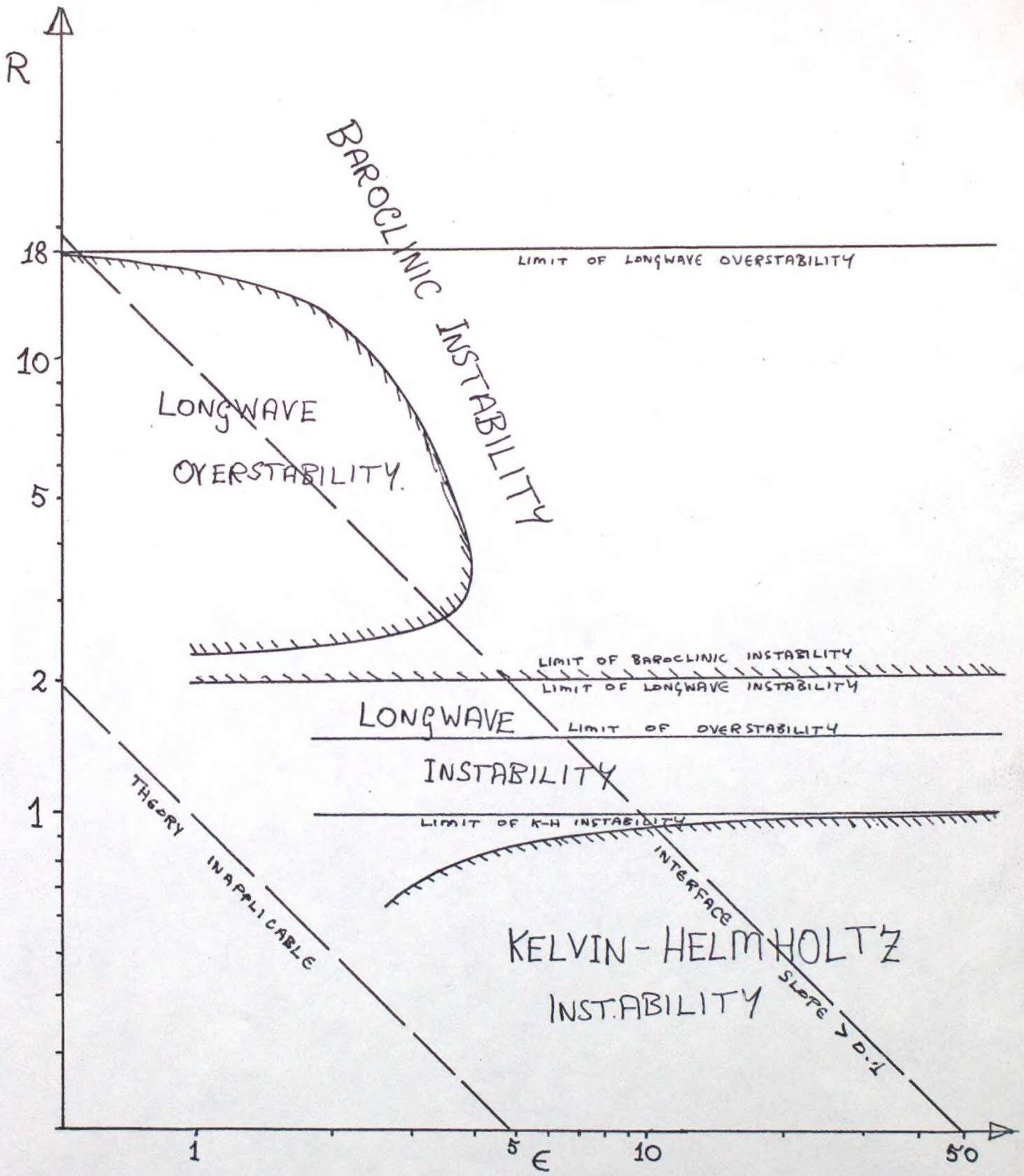

Fig (10): Regime diagram for two layer system when T=0.01 and σ=0.

The solid lines delimit the regions where various instabilities occur, and the hatched lines regions where they dominate.